

# Nucleation barriers in tetrahedral liquids spanning glassy and crystallizing regimes

Ivan Saika-Voivod,<sup>1,a)</sup> Flavio Romano,<sup>2</sup> and Francesco Sciortino<sup>3</sup>

<sup>1</sup>*Department of Physics and Physical Oceanography, Memorial University of Newfoundland, St. John's, Newfoundland A1B 3X7, Canada*

<sup>2</sup>*Dipartimento di Fisica, Sapienza – Università di Roma, P.le A. Moro 5, 00185 Roma, Italy*

<sup>3</sup>*Dipartimento di Fisica and CNR-ISC, Sapienza – Università di Roma, P.le A. Moro 5, 00185 Roma, Italy*

(Received 20 June 2011; accepted 24 August 2011; published online 27 September 2011)

Crystallization and vitrification of tetrahedral liquids are important both from a fundamental and a technological point of view. Here, we study via extensive umbrella sampling Monte Carlo computer simulations the nucleation barriers for a simple model for tetrahedral patchy particles in the regime where open tetrahedral crystal structures (namely, cubic and hexagonal diamond and their stacking hybrids) are thermodynamically stable. We show that by changing the angular bond width, it is possible to move from a glass-forming model to a readily crystallizing model. From the shape of the barrier we infer the role of surface tension in the formation of the crystalline clusters. Studying the trends of the nucleation barriers with the temperature and the patch width, we are able to identify an optimal value of the patch size that leads to easy nucleation. Finally, we find that the nucleation barrier is the same, within our numerical precision, for both diamond crystals and for their stacking forms. © 2011 American Institute of Physics. [doi:10.1063/1.3638046]

## I. INTRODUCTION

Crystallization is central to several fields, from materials research to biological science, not to mention its technological relevance.<sup>1,2</sup> Several human pathologies are also caused by crystal nucleation in protein solutions.<sup>3</sup> Understanding crystal nucleation requires both the evaluation of the stability fields of the fluid and crystal phases (i.e., knowledge of the chemical potentials of all possible phases), as well as the evaluation of the thermodynamic barriers controlling the formation of the stable phase from the metastable one and of the kinetic prefactors fixing the time scale of the diffusional processes, all key quantities on which the nucleation rate depends.

In recent years, several numerical methodologies have been developed for accurately evaluating phase diagrams from the free energies of the fluid and crystal phases. We refer the reader to the review by Vega and co-workers.<sup>4</sup> Also for crystallization, various methods are now available for calculating free energy barriers and nucleation rates,<sup>5–9</sup> making it possible to generate accurate data for model potentials and, more importantly, to compare the nucleation rate obtained numerically with theoretical predictions, mostly based on classical nucleation theory (CNT),<sup>10–15</sup> as well as with experimental data when possible.

One of the main motivations for the development of the special methods for studying nucleation is the proper sampling of the equilibrium cluster size distribution  $N(n)$  within the metastable liquid, i.e., the number of crystal-like clusters composed of  $n$  particles. The work of forming a cluster of size

$n$  from the liquid is given in terms of  $N(n)$  by<sup>8</sup>

$$\beta \Delta G(n) = -\ln \left[ \frac{N(n)}{N_p} \right], \quad (1)$$

where  $N_p$  is the number of particles in the system and  $\beta \equiv (k_B T)^{-1}$ , where  $T$  is the temperature and  $k_B$  is the Boltzmann constant. Below the melting temperature,  $\beta \Delta G(n)$  has a maximum value  $\beta \Delta G^*$  at a critical nucleus size  $n^*$ .  $\beta \Delta G^*$  enters into the expression for the rate of nucleation exponentially, and is therefore the main consideration in determining the rate from a thermodynamic perspective. Very generally, the larger the difference in chemical potential between liquid and crystal  $\Delta\mu$ , often referred to as the driving force for crystallization, the smaller  $\beta \Delta G^*$  is. Conversely, the surface tension  $\gamma$  between crystallite and surrounding liquid always acts against the growth of crystallites, and so  $\beta \Delta G^*$  increases with  $\gamma$ . Hence, the ability of a system to crystallize is governed by the interplay between  $\Delta\mu$  and  $\gamma$ . Within CNT, this relationship is captured through  $\Delta G^* \propto \gamma^3 / (\rho_x |\Delta\mu|)^2$ , where  $\rho_x$  is the number density of the cluster and the proportionality constant depends on its shape.

Recently, simulation studies have begun to address crystallization of tetrahedral liquids.<sup>16–21</sup> This class of interesting liquids includes biological and technologically important molecular and atomic materials, such as water, silica, silicon, and carbon. One common feature in these systems is the formation of open, low density structures such as the diamond cubic (DC) crystal. For carbon, simulations have shown the importance of the liquid structure in governing nucleation barriers.<sup>22,23</sup> In a generalized form of the Stillinger-Weber model for silicon,<sup>24</sup> the degree of tetrahedrality was shown to have a strong impact on DC nucleation and its interrelation with the appearance of a metastable liquid–liquid critical point.<sup>25</sup> Further, for silicon and germanium, the lower density

<sup>a)</sup> Author to whom correspondence should be addressed. Electronic mail: saika@mun.ca.

of the DC crystal with respect to the liquid was shown to give rise to a preference for nucleation near the surface, with similar implications for water.<sup>26</sup> The self-assembly of a DC colloidal crystal is also of interest in the field of photonics, since such an ordered structure of dielectric spheres is expected to exhibit a band structure with a large gap within the visible wavelengths of light.<sup>27</sup>

Tetrahedral liquids are interesting from another perspective as well. Often, in these systems crystal formation is inhibited by the onset of a glassy behavior which dramatically slows down the microscopic dynamics, thus preventing the transition to the ordered structure. The glass forming ability of silica and the ease with which water crystallizes stand in stark contrast to each other.

Motivated by these issues of scientific and technological interest, recently, some of us<sup>28</sup> have thoroughly investigated the question of how to best design tetrahedral patchy colloidal particles that spontaneously assemble into open crystal structures through computer simulations of the Kern-Frenkel model.<sup>29</sup> It was shown that the angular width of the patch plays a key role in determining if the system, at low temperatures, forms a disordered glass structure or a crystal, a result which may also be of interest for interpreting the glass-forming ability of atomic and molecular systems. When the patch width is small, the crystal coexists with a fluid and  $\beta|\Delta\mu|$  (the driving force for crystallization) increases quickly with undercooling, while when the patch width is large, the crystal coexists with a fully bonded liquid state and  $\beta|\Delta\mu|$  grows only moderately with undercooling. It was also shown that the model spontaneously forms a crystal composed of a mixture of two open tetrahedral structures, the DC and the diamond hexagonal (DH) crystals, and that the chemical potentials for the two polymorphs were indistinguishable within the precision of the calculations.

In this article we proceed one step further by investigating, for the same tetrahedral model, the patch width dependence of the free energy barrier to nucleating the DC and/or DH crystals. Interestingly, we find that, at comparable undercooling, the barrier height  $\beta\Delta G^*$  does not monotonically decrease with the increasing patch width as one would expect from a consideration of  $\beta|\Delta\mu|$  alone. Indeed, comparing the barrier shape with CNT predictions, we find that the surface tension  $\gamma$  increases on decreasing the patch width, a result that we tentatively connect to the larger structural and density difference between fluid and crystal. We do find that for narrow patches,  $\beta\Delta G^*$  generally shows a strong  $T$  dependence, rapidly decreasing to a homogenous nucleation limit, while for wide patches,  $\beta\Delta G^*$  decreases more slowly with decreasing  $T$ , allowing the system to reach the glassy regime. Additionally, at the widest patch studied, the barriers remain very large (of the order of  $50 k_B T$ ) even for significant undercooling. This confirms that despite the benefit of a lower surface tension, the lack of a buildup of a large difference in chemical potential is mainly responsible for disfavoring crystallization of particles with wide patches. The presented results confirm that DC/DH will spontaneously form when the angular width of the patch is sufficiently small.

The remainder of this article is organized as follows. In Sec. II, we outline our criteria for defining crystal-like clus-

ters and the umbrella sampling Monte Carlo (MC) procedure for calculating nucleation barriers. In Sec. III, we present our results, including a fairly detailed examination of the robustness of  $\beta\Delta G^*$  to varying the cluster-defining criteria and the dependence of  $n^*$  and cluster composition (e.g., percentage of DC particles) on them. We then present our summary and conclusions in Sec. IV.

## II. METHODS

We perform biased Monte Carlo simulations<sup>33</sup> at constant  $T$  and pressure  $P$  of the Kern-Frenkel model<sup>29</sup> with  $N_p = 1000$  particles, each with hard sphere diameter  $\sigma$ , and each having four tetrahedrally arranged attractive patches of the range  $\delta = 0.24\sigma$ , strength  $u_0$ , and angular width  $2\theta$ .<sup>28,34</sup> We report  $T$  and  $P$  as dimensionless quantities, after rescaling by  $u_0/k_B$  and  $u_0/\sigma^3$ , respectively. We investigate four different values of  $\theta$ , namely, those corresponding to  $\cos\theta = 0.98$ , 0.96, 0.94, and 0.92 ( $\theta = 11.5^\circ$ ,  $16.3^\circ$ ,  $19.9^\circ$ , and  $23.1^\circ$ ). For the value of  $\delta$  we use the condition  $\cos\theta > 0.9151$  which guarantees that a patch can only accommodate a single bond, and therefore the maximum number of bonds per particle is restricted to four.<sup>34</sup>

Figure 1 shows the phase diagrams for the Kern-Frenkel models we study here, obtained either directly from Ref. 28 [panels (a) and (d)] or by extending the calculations to cases not reported in that work. The phase diagrams show high and low density fully bonded crystal phases, in which each particle is bonded with four neighbors (i.e., the energy per particle is  $-2u_0$ ). The low density crystal is an open tetrahedral structure and it can exist in two polymorphs, DC and DH. As noted in Ref. 28, the chemical potentials for the DH and DC structures are largely indistinguishable, and indeed it has been observed that when the liquid crystallizes spontaneously to the open tetrahedral structure, it does so by forming a stacking of DC and DH planes.<sup>28</sup> Indeed, DH and DC crystalline layers can stack in an analogous way to the fcc/hcp stacking in

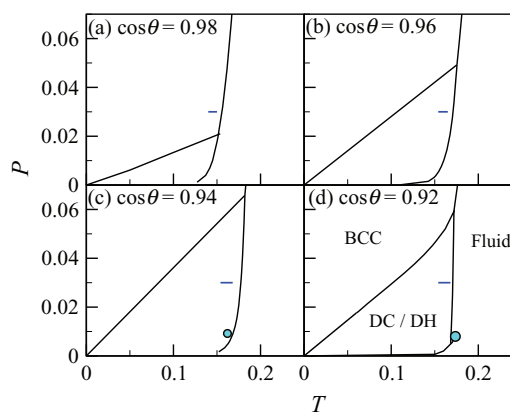


FIG. 1. Equilibrium phase diagrams for all the models studied in the low  $P$ , low  $T$  region, where the open crystal structures are stable. The short blue lines correspond to the temperatures for which the nucleation barriers have been investigated. The circles mark the gas–liquid critical point. For the narrow patch models [(a) and (b)], nucleation is so effective that the location of the critical point cannot be properly estimated. However, we have checked that the studied isobar is located significantly above the critical pressure. Phase diagrams in (a) and (d) are taken from Ref. 28.

hard-spheres. The dense phase, composed of two interpenetrating fully bonded DC structures, is a body centered cubic (bcc) crystal. The fluid separates into gas and liquid phases below the critical temperature. Since the range of the potential is short compared to the particle size, the critical point is almost always metastable with respect to the crystal phase.

In the following, we study the crystallization barriers to the DC/DH crystal at one selected pressure. Specifically, we choose  $P = 0.03$  in order to avoid interference with gas-liquid phase separation. For all the models studied, with the exception of  $\cos\theta = 0.98$ , the most stable phase at that pressure is the open tetrahedral crystal. In the case of  $\cos\theta = 0.98$ , bcc is the stable phase at this pressure, but as previous studies have shown, spontaneous crystallization results always in the open structure,<sup>28</sup> an example of the Ostwald step rule.<sup>30-32</sup>

The nucleation to tetrahedral crystals has been studied previously in simulations<sup>22,23,26</sup> and we follow the established methodology to evaluate the free energy barriers. A novel issue arises from the presence of two crystals with different symmetries in the same stability field, as we discuss in the following.

We use Steinhardt bond order parameters<sup>35</sup> based on spherical harmonics of order  $l = 3$ . For each particle we define the complex vector

$$q_{lm}(i) = \frac{1}{N_b(i)} \sum_{j=1}^{N_b(i)} Y_{lm}(\hat{r}_{ij}), \quad (2)$$

where the sum is over the  $N_b(i)$  neighbors of particle  $i$ , defined as those particles within a distance of  $(1 + \delta)\sigma = 1.24\sigma$  of particle  $i$ . The dot product

$$c_{ij} = \sum_{m=-l}^l \hat{q}_{lm}(i) \hat{q}_{lm}^*(j), \quad (3)$$

where

$$\hat{q}_{lm}(i) = q_{lm}(i) / \left( \sum_{m=-l}^l |q_{lm}(i)|^2 \right)^{1/2} \quad (4)$$

and  $\hat{q}_{lm}^*(i)$  is its complex conjugate, determines the degree of orientational correlation between neighboring particles  $i$  and  $j$ . Figure 2 shows the  $c_{ij}$  distributions for the fluid and the DC and DH crystals. The DC distribution is peaked around  $c_{ij} = -1$  only, while the DH crystal also shows a peak near  $c_{ij} = -0.1$ . In the DH crystal, each particle has three neighbors with  $c_{ij} \approx -1$  and one with  $c_{ij} \approx -0.1$ , while in the DC crystal, all four bonded neighbors have  $c_{ij} \approx -1$ . This provides a local basis for distinguishing particles as being DC or DH. The fluid distributions are very wide and show sharp peaks for large values of  $\cos\theta$  (small bonding angles). The peaks become more intense on heating, which we attribute to a lower density and higher energy; we identify the peaks as signals of specific geometrical assemblies in the fluid with unfilled bonds. For example, a dimer has  $c_{ij} = -1$ , while both bonds in a trimer have  $c_{ij} = -0.82$ .

The possibility of separating the  $c_{ij}$  ranges in which crystal-like or fluid-like particles are mostly contributing offers a way of associating a value of  $c_{ij}$  with a local

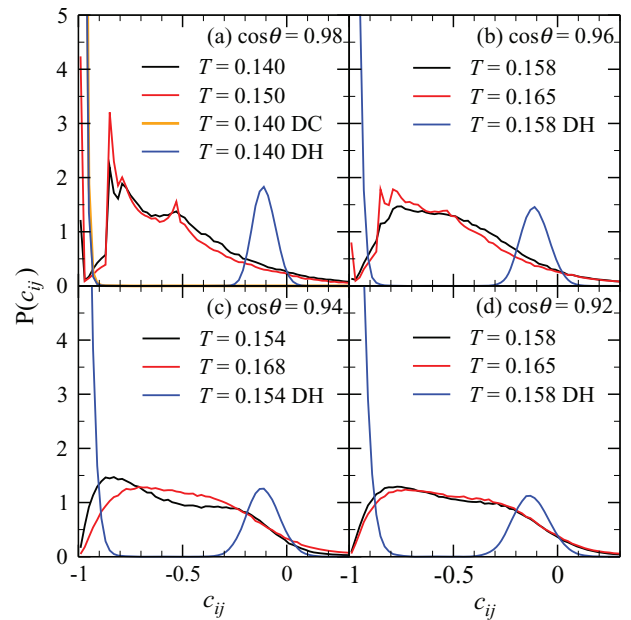


FIG. 2. Probability distributions of the dot product  $c_{ij}$  in the liquid and crystal structures. The distribution for DC, shown only in panel (a), is a single peak near  $-1$  and is nearly indistinguishable from the DH peak at  $-1$  on the scale of the plots. The distributions for the crystals do not vary significantly over our  $T$  range.

structure (crystal or fluid). Usually, a threshold number of crystal-like connections is selected to distinguish particles as being fluid-like or crystal-like. In the following, we start by defining a crystal-like connection between neighbors as the one with  $c_{ij} < q_u$ , with  $q_u = -0.87$ , and a crystal-like particle as the one which has three or more crystal-like connections. This definition does not allow one to discriminate between DC and DH, and hence appears to be a reasonable first step in the investigation of the nucleation barriers.<sup>22,23,26</sup> We complement this study with an additional investigation where we differentiate between DC and DH by requiring that a solid-like particle has four neighbors with  $c_{ij} < -0.87$  in the DC case or three neighbors with  $c_{ij} < -0.87$  and one with  $-0.3 < c_{ij} < 0.1$  in the DH case. For completeness, we probe three cases: (i) the case where the growing crystal is composed only of DC particles; (ii) the case where the growing crystal is composed only of DH particles; (iii) the case where the growing crystal is composed of DC or DH particles.

We follow the standard methodology for defining a biasing potential which helps the formation of crystalline clusters. To this aim we add to the Kern-Frenkel potential a perturbation given by

$$\phi = \kappa(n_{\max} - n_0)^2, \quad (5)$$

where  $\kappa$  is a suitably chosen constant that controls the range of sampled crystal cluster sizes, centered near  $n_0$ , and  $n_{\max}$  is the size of the largest crystalline cluster in the system. Depending on the steepness of  $\Delta G(n)$ , we adjust the value of  $\kappa$  to obtain good sampling, but for almost all simulations,  $\kappa = 0.075$ . To define a crystal-like cluster, we state that two neighboring crystal-like particles are part of the same cluster.

New configurations in the umbrella sampling (US) MC chains are generated as follows. Given a starting

configuration with largest cluster  $n_{\max}^0$ , we perform a trajectory of 20 Metropolis MC steps, where one such step is on average  $N_p - 1$  particle translations and rotations and one volume change, in order to arrive at a configuration with largest cluster  $n_{\max}^1$ . The new configuration is accepted with probability  $\min(1, \exp\{-\beta[\phi(n_{\max}^1) - \phi(n_{\max}^0)]\})$ . If the new configuration is accepted, it becomes the starting point for the next MC trajectory. If it is rejected, the entire trajectory is discarded and the  $n_{\max}^0$  configuration is kept and used as the starting point for generating another MC trajectory. For the slowest state points, we perform  $10^7$  US attempts. We perform several US simulations for different values of  $n_0$ . Generally, two adjacent US windows are spaced by  $\Delta n_0 = 3$  to ensure good sampling of the reaction path. For each US window we then evaluate the solid cluster size distribution  $\tilde{N}(n)$  and  $P_{\max}(n)$ , the probability that the largest cluster in the system is of size  $n$ .

The cluster size distribution  $N(n)$  in the  $NPT$  ensemble for each window is worked back from the biased ensemble as in Ref. 8 with

$$N(n) = \langle \exp[\beta\phi(n_{\max})] \tilde{N}(n) \rangle_{\text{biased}} \quad (6)$$

up to a multiplicative constant, where  $\langle \dots \rangle$  indicates an ensemble average. Portions of  $\beta\Delta G(n)$  are determined from simulations at different values of  $n_0$  up to additive constants, in agreement with Eq. (1). These pieces are matched by minimizing the difference between overlapping portions after discarding data for which  $P_{\max}(n)$  is less than 0.01 (to ensure good sampling). Alternatively, we find the free energy difference  $\Delta G(n) - \Delta G(n-1)$  as a weighted average of the values obtained with simulations at different  $n_0$  in which clusters of size  $n$  and  $n-1$  have been sampled, where the weight is given by  $\exp[-2k(n-n_0)]$ . As a result  $\Delta G(n) = \sum_{j=1}^n [\Delta G(j) - \Delta G(j-1)]$ . The two procedures give equivalent results. We then shift the curves so that  $\Delta G(0) = 0$ . While this is not formally correct, since the number of liquid-like particles  $[N(0)]$  is not precisely equal to  $N_p$ , the error is negligible (of the order of  $0.01 k_B T$  or less). We stress here that at this stage we do not differentiate between DH and DC particles. We have checked that indeed the largest crystalline cluster is a mixture of the two crystal local structures. We will address this point in more detail later on.

To ensure independence of the initial conditions, we construct our barriers starting from two different sets of data. In the first set we use the biasing potential to grow clusters in the fluid, starting the US simulation at  $n_0$  from a configuration extracted from the previous windows. In the second set, we seed the biased simulations at  $\cos\theta = 0.98$  with crystallite-containing configurations from homogeneously nucleating unbiased MC runs at  $\cos\theta = 0.98$ . Configurations from equilibrated runs at  $\cos\theta = 0.98$  are then used to seed simulations at  $\cos\theta = 0.96$  at high  $T$ , with the idea that on increasing the width of the patch, the bonds present in the  $\cos\theta = 0.98$  configurations will be at least initially maintained at  $\cos\theta = 0.96$ . Thus, we hope to never stray too far out of equilibrium. Equilibrated configurations from  $\cos\theta = 0.96$  are then used to seed simulations at  $\cos\theta = 0.94$ , and then similarly for  $\cos\theta = 0.92$ .

### III. RESULTS

#### A. Barrier profiles

In Fig. 3 we show our results for the  $\Delta G(n)$  profiles for the four models of different patch widths at various  $T$ . The range of  $T$  where the barrier can be calculated with the present methodology is restricted both from above and below for different reasons. At large  $T$  (small supercooling), the critical nucleus is large compared to the system size. At low  $T$ , different reasons conspire against a proper evaluation of the barrier height. For example, in the case  $\cos\theta = 0.92$ , the slow kinetics associated with the proximity of a glass transition prevent proper equilibration already at temperatures where the critical nucleus is of comparable size to the studied system. In this same case, it has been suggested on the basis of the explicit evaluation of the difference in chemical potential between the crystal and the fluid that, at odds with the standard behavior, barriers do not grow with further supercooling.<sup>28</sup> The difficulty of evaluating barriers for the wide patch model is consistent with this proposition. In the case of narrow patches,  $\cos\theta = 0.98$ , we are limited to a barrier height of the order of  $30 k_B T$ . For lower  $T$ , despite slow dynamics not being an issue, the results of the calculations become more and more affected by the presence of secondary crystal clusters. While in theory the presence of more than one cluster is not a problem, in our opinion this effect highlights an incorrect definition of crystallinity at the local level, which artificially breaks a single cluster into two (or more) pieces. Hence, at the lowest  $T$ , the barrier calculations become difficult owing to the appearance of clusters of comparable size to the largest one in the system. A visual inspection of configurations confirms the formation of secondary clusters occurring next to the

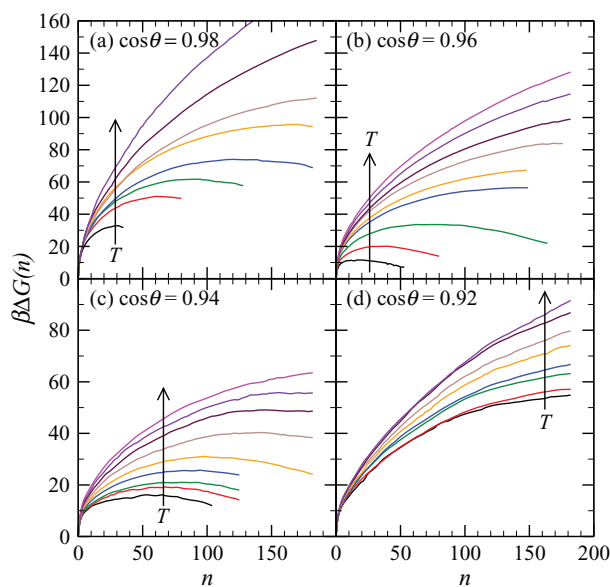


FIG. 3. Nucleation barriers  $\beta\Delta G(n)$  for various bond angular widths and temperatures. Panel (a)  $\cos\theta = 0.98$ , from bottom to top  $T = 0.140, 0.142, 0.143, 0.144, 0.145, 0.146, 0.148, 0.150$ . Panel (b)  $\cos\theta = 0.96$ , from bottom to top  $T = 0.154, 0.156, 0.158, 0.160, 0.161, 0.162, 0.163, 0.164, 0.165$ . Panel (c)  $\cos\theta = 0.94$ , from bottom to top  $T = 0.154, 0.156, 0.158, 0.160, 0.162, 0.164, 0.166, 0.167, 0.168$ . Panel (d)  $\cos\theta = 0.92$ , from bottom to top  $T = 0.154, 0.156, 0.158, 0.160, 0.162, 0.164, 0.166, 0.168$ .

primary one, separated by particles that fall outside the cutoffs defining crystal-like particles.

This problem, most noticeable for  $\cos\theta = 0.98$  but occurring for other models at low enough  $T$ , does depend on the choice of  $q_u$ . A closer examination of Fig. 2 reveals that the  $c_{ij}$  value at which the liquid and crystal distributions cross moves progressively toward more positive values as  $\cos\theta$  decreases, attaining a value of  $-0.87$  only at  $\cos\theta = 0.92$ . However, rather than changing  $q_u$  for each model, we keep the same value for uniformity, but then separately explore the effects of varying  $q_u$  below, at least for  $\cos\theta = 0.98$ .

We recall that for a proper evaluation of the barriers in the low  $T$  limit, where homogeneous nucleation is taking place, one can apply the methodology based on mean first-passage times.<sup>36–40</sup> We note that we have checked the quality of our calculations for state points where the barrier is of the order of  $20k_B T$  by comparing the US results with  $N(n)$  evaluated in unconstrained simulations.

While we will discuss the role of  $\beta|\Delta\mu|$  on our barriers below, we stress that only partial insight into the  $T$  dependence of the barriers can be gained by considering the behavior of  $\beta\Delta\mu$  for the different models, shown in Fig. 7.

Although we do not perform any quantitative analysis of the shape of the clusters, we can say that they are generally compact and isotropic, with fairly obvious facets. This assessment is based on a visual survey spanning the range in  $\cos\theta$  of several configurations containing clusters 60–150 particles in size.

## B. Fits

Within the phenomenological framework of CNT, the work of forming an  $n$ -sized cluster can be written as

$$\beta\Delta G(n) = -\beta|\Delta\mu|n + \beta\gamma A, \quad (7)$$

where  $A$  is the surface area of the cluster. We therefore fit our profiles to

$$\beta\Delta G(n) = -an + bn^{2/3}, \quad (8)$$

where  $a = \beta|\Delta\mu|$  and  $b \sim \beta\gamma$  and we have assumed a compact cluster. Below, we compare our results for  $a$  against  $\beta|\Delta\mu|$ , as some studies suggest a very good correspondence,<sup>8,9,41</sup> and justify our assumption that  $b$  is equal to  $\beta\gamma$  up to a constant factor which depends on the shape and density of the crystallites. Recently, it has been shown for a soft-core colloidal model that the procedure we follow here for determining  $n$  may not be sufficient for describing crystal-like structures, but that the scaling represented by Eq. (8) may still hold, i.e., changing the parameters used to define a crystalline cluster will change the numerical values of  $a$  and  $b$ .<sup>42</sup> We explore this in some detail below.

We show two representative  $\beta\Delta G(n)$  curves along with fits to Eq. (8) in Fig. 4. While there is a deviation between the data and fits at small  $n$ , the overall description is rather good. Moreover, the values for  $n^*$  and  $\Delta G^*$  extracted from the fits coincide with those obtained directly from the barriers. Improvement of the small  $n$  description could be accomplished along the lines suggested in Ref. 43 but it is outside the scope of the present work.

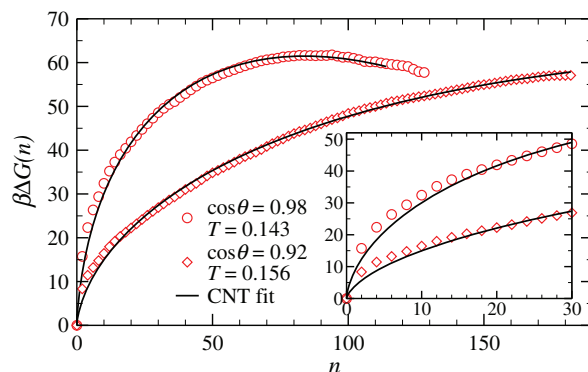


FIG. 4. Fits of two of the barrier profiles studied to the CNT form (Eq. (8)). For the  $\cos\theta = 0.98$  curve,  $a = 1.47$  and  $b = 9.64$ , and for  $\cos\theta = 0.92$ ,  $a = 0.405$  and  $b = 4.10$ . While there is a deviation at small  $n$ , the overall representation of the curve is fairly good, especially in terms of the barrier height  $\Delta G^*$  and size of the critical nucleus  $n^*$ . Inset: low- $n$  region of the same data, highlighting the deviation from the CNT form.

The fits allow us to plausibly extrapolate our  $\Delta G(n)$  profiles to values of  $n$  larger than what we can simulate in our  $N_p = 1000$  system, allowing us to estimate  $n^*$  and  $\beta\Delta G^*$  for all the  $T$  that we study. While we do not rely strongly on the accuracy of the extrapolations, they do provide a stronger sense of the trends in the data.

The numerical values of the fit parameters require further exploration to understand, as we do below. For example, for the  $\cos\theta = 0.98$  curve shown in Fig. 4, the parameter  $a = 1.47$ , while  $\beta|\Delta\mu| = 0.790$ , a sizable discrepancy for two quantities that are the same, in principle.

## C. $T$ dependence of $\Delta G^*$ and $n^*$

Figure 5(a) shows  $\beta\Delta G^*$  as a function of  $T/T_m$ , where  $T_m$  is the melting temperature for the four models<sup>45</sup> [( $\cos\theta$ ,  $T_m$ ): (0.98, 0.153), (0.96, 0.169), (0.94, 0.172), (0.92, 0.174)]. For small angles, the  $T$  dependence of  $\beta\Delta G^*$  is significant, and can be modeled rather well in the present range of barriers with an exponential function. The fast decrease of  $\beta\Delta G^*$  provides evidence for the inevitability of crystallization. For larger angles, we observe both a significant change in slope, i.e., a much slower decrease of the barrier height with supercooling, as well as a progressive increase of the barrier height at fixed supercooling with increasing angle. The trend is accounted for by the results reported in Ref. 28, namely, that  $\beta|\Delta\mu|$  becomes a weaker function of temperature as  $\theta$  increases. On the basis of the results presented in Fig. 5(a), the model with  $\cos\theta = 0.96$  appears to be the optimal candidate for crystallization from a thermodynamic perspective, since modest supercooling is sufficient to induce barriers of height of the order of  $10k_B T$ .

Figure 5(b) shows  $n^*$  as a function of  $T/T_m$ , showing similar trends as for  $\beta\Delta G^*(T)$ . The  $\cos\theta = 0.98$  and  $0.96$  models are similar, attaining small  $n^*$  for a relatively small degree of supercooling, while the models with wider patches seem to require larger sizes of critical nuclei as  $T$  decreases. The  $T$  dependence of  $n^*$  is much flatter, suggesting that the

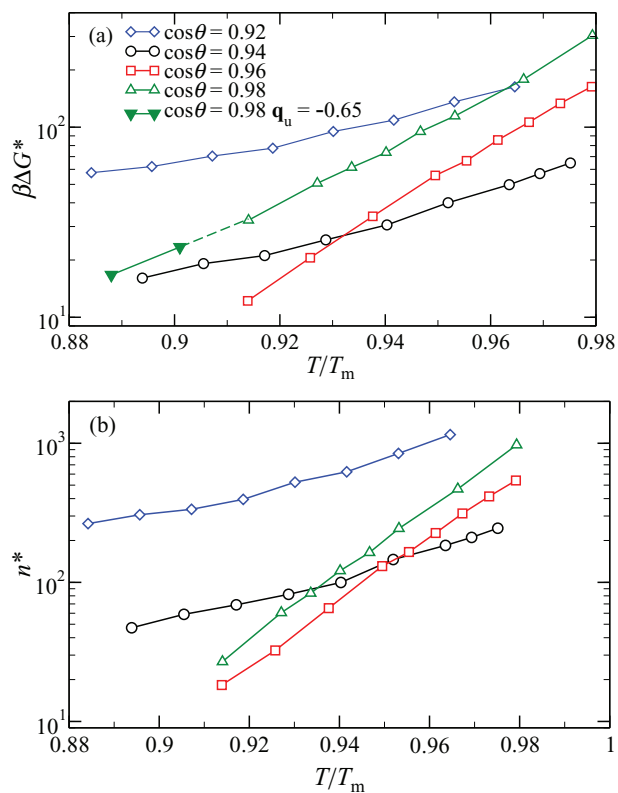


FIG. 5. (a) Barrier height  $\beta\Delta G^*$  as a function of  $T/T_m$ . For high values of  $\cos\theta$ , the barrier decreases significantly with decreasing temperature, while the slope is much more shallow for low values of  $\cos\theta$ . The two points at lowest  $T$  for  $\cos\theta = 0.98$  are obtained from US simulations employing a more relaxed  $c_{ij}$  cutoff of  $q_u = -0.65$  after checking for consistency at higher  $T$ . (b) Critical cluster size  $n^*$  as a function of the reduced temperature. Also in this case, the trend with  $T$  is stronger in narrow-patch models than in wide-patch models.

critical nucleus remains significantly large even under deep supercooling.

#### D. Surface tension

To illustrate the dependence of the surface tension on the patch width, motivated by the relation  $3\beta\Delta G^* = bn^{*2/3}$  that follows from Eq. (8), we plot in Fig. 6(a)  $\beta\Delta G^*$  as a function of  $n^{*2/3}$ . For all models, a reasonable linear dependence is observed, with a slope that progressively increases with  $\cos\theta$  beyond 0.94. This results in a larger critical size for a given barrier height as the patch width increases. The near linearity also suggests that the surface tension does not have a strong dependence on supercooling. In Fig. 6(b) we show  $b$  as a function of  $T/T_m$  as obtained from the fitting procedure for the different state points studied. The surface tension increases significantly on decreasing the angular patch width. Once again, however, the two models with the largest patches are quite similar in their behavior.

It is worthwhile noting that the densities at our simulated  $P$  for these two wide patch models (at our lowest  $T$ ) are very similar with values near  $\rho\sigma^3 = 0.47$ , almost matching the crystal density (where  $\rho$  is the number density). The density is smaller for  $\cos\theta = 0.96$ , and smallest for  $\cos\theta = 0.98$ . Thus, the values of  $b$  for the different models appear to reflect the

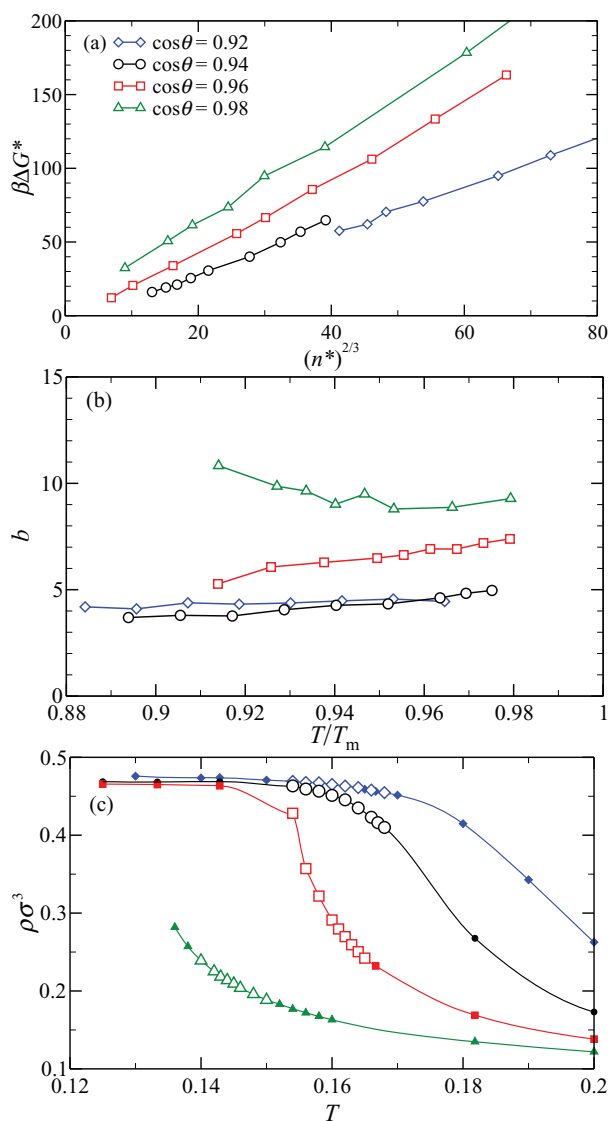


FIG. 6. (a) Barrier height as a function of  $n^{*2/3}$  (proportional to the surface area of the cluster). All models show a linear behavior. (b) Surface coefficient  $b$  of the CNT fit as a function of the reduced temperature. The surface term does not change significantly with  $T$ , as compared to the barrier height [see Fig. 5(a)]. (c) Reduced number density  $\rho\sigma^3$  as a function of  $T$  at  $P = 0.03$  for the models studied. For all panels, open symbols correspond to the same state points for which the barriers in Fig. 3 are calculated. Curves are a guide to the eye.

differences in density, with a better match in density between fluid and crystal giving rise to a smaller surface tension. However, a plot of the  $T$  dependence of the densities in Fig. 6(c) shows that density does not solely determine  $b$ , as indicated by the variation of density without a correspondingly large variation in  $b$  within each model.

#### E. $a$ vs $\beta\Delta\mu$

In Fig. 7 we plot  $\beta|\Delta\mu|$  (Ref. 45) and  $a$  (obtained from the CNT fits) as functions of  $T$ . For comparison purposes, all the values of  $a$  appearing in the figure have been multiplied by a factor of 0.4, i.e., the values of  $a$  are significantly higher than those expected from independent calculation of  $\beta|\Delta\mu|$ . However, it is quite comforting that the rescaled  $a$  matches

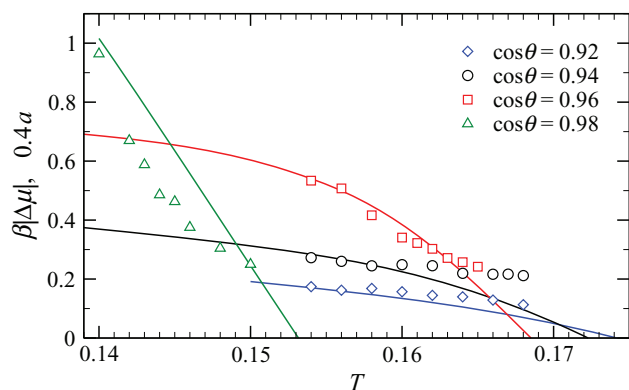


FIG. 7. CNT bulk fit parameter  $a$  as a function of temperature (points) compared with the difference in chemical potential  $\beta|\Delta\mu|$  (lines). While the two quantities show similar trends, to achieve quantitative agreement we multiply values of  $a$  in the plot by a universal scaling factor of 0.4.

$\beta\Delta\mu$  quite well across  $T$  and  $\theta$ , as this strengthens our assumption that the fit parameter  $b$  is proportional to  $\beta\gamma$  with the same proportionality constant across all the models.

On the other hand, it is somewhat perplexing that such a large rescaling is required at all. In a few previous studies, comparison between  $a$  and  $\beta\Delta\mu$  has shown that in some cases a close correspondence is observed,<sup>8,9,41</sup> while, in principle, the value of  $a$  should vary with the definition crystal-like particles. There are several potential reasons why such a disagreement can be found. First of all, the assumption of CNT may not be fully satisfied, including those concerning the structure of the crystallites and the sharpness of the interface.<sup>42</sup> Second, an imperfect classification of particles as solid-like leads to an imperfect evaluation of the cluster size and a classification-dependence of  $a$  and  $b$ .

As a test of this second hypothesis and to illustrate the effect of the parameters chosen to define crystalline clusters, we plot in Fig. 8 sets of barrier profiles obtained for  $\cos\theta$

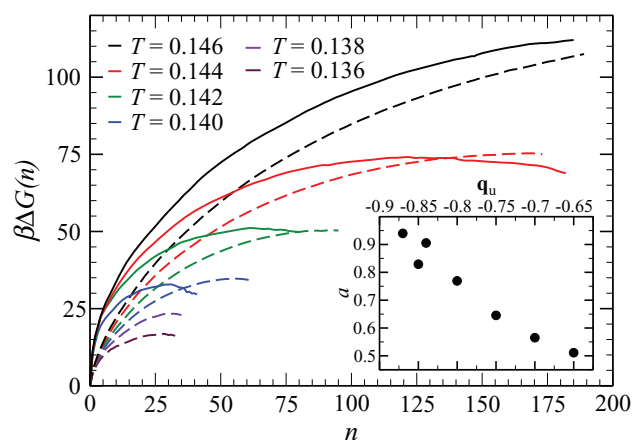


FIG. 8. Comparison of the nucleation barriers obtained with two different order parameters,  $q_u = -0.65$  (dashed lines) and  $q_u = -0.87$  for the  $\cos\theta = 0.98$  model. As expected, the barrier heights are consistent (see Ref. 44), but the critical cluster sizes differ significantly. The more relaxed order parameter leads to a larger critical cluster, possibly due to the fact that it includes more particles on the surface. In the inset we also show the dependence of the bulk CNT term  $a$  as a function of the order parameter, showing that it increases by making the order parameters more strict.

$= 0.98$  using  $q_u = -0.65$  compared against using  $q_u = -0.87$ . While  $\Delta G^*$  remains invariant to within error with respect to  $q_u$ , at all investigated  $T$ ,  $n^*$  increases, as expected, for smaller values of  $q_u$ . Estimates for  $n^*$ , with an uncertainty of roughly  $\pm 10$  or less unless otherwise indicated, for the  $T = 0.140, 0.142, 0.144$ , and  $0.146$  curves shown in Fig. 8 are 27, 61, 121, and 244, respectively, for  $q_u = -0.87$ , while they are 55, 93, 177, and  $428 \pm 80$  for  $q_u = -0.65$ . In other words, the size of the critical nucleus is strongly dependent on the criteria chosen to define solid-like particles. It is not a surprise that  $\Delta G^*$  is a much more robust value, since the work required to produce the critical nucleus is independent on how the cluster is described. In other words, the “real” critical nucleus (i.e., configurations which 50% of the time will crystallize and 50% will melt again into a fluid state) is what needs to be sampled in the simulation. The number of particles that compose this cluster depends on the definition, affecting the perceived size, but not the barrier height. These conclusions are in agreement with the work of Filion *et al.*<sup>44</sup> on spherical particles.

In the inset of Fig. 8, we show  $a$  as a function of  $q_u$  for  $T = 0.146$  and  $\cos\theta = 0.98$ , and we see that  $a$  varies by roughly a factor of 2 for the reasonable range of  $q_u$  we have explored. Coincidentally, the value for  $\beta|\Delta\mu|$  for this state point is 0.56. Thus, for an appropriate choice of  $q_u$ , Eqs. (7) and (8) describe the nucleation barrier profiles both in scaling and in the numerical value of  $\Delta\mu$ , but how to choose the appropriate  $q_u$  *a priori* is not clear.

The more inclusive choice of  $q_u = -0.65$  allows one to more easily explore the regime of low barrier heights, less hampered by the formation of secondary clusters. Using  $q_u = -0.65$ , we are able to add two additional points to the curve for  $\cos\theta = 0.98$  in Fig. 5(a).

## F. DH vs DC

As we have alluded to before, the clusters are formed by a mixture of local DC and DH particles. Indeed, the criterion of having at least three connected neighbors ( $c_{ij} < q_u$ ) for defining solid-like particles, accepts either a locally DC or DH particle as solid. However, this definition is more likely to misidentify a DH-like particle as liquid-like, since particles in the DC crystal have four such connections, while DH particles only have three. The biasing potential may therefore tend to grow clusters richer in DC than would occur naturally. In the following, we therefore compare this criterion with other criteria which enforce the growth of pure DC, pure DH, or an unbiased mixture of the two. We do this at  $\cos\theta = 0.98$ , where the calculations are the fastest.

For pure DC, we retain  $q_u = -0.87$  and simply require that the number of connections be exactly four (as opposed to at least three). With this more restrictive criterion, the solid-like particles must have a DC environment. For pure DH, we require exactly three connections with  $c_{ij} < q_u = -0.87$  and one connection with  $-0.3 < c_{ij} < 0.1$ . In this way, DC particles are excluded and cannot participate in crystalline clusters. For the mixed DH/DC case, a particle is solid-like if it is determined again by exactly four connections, but this time

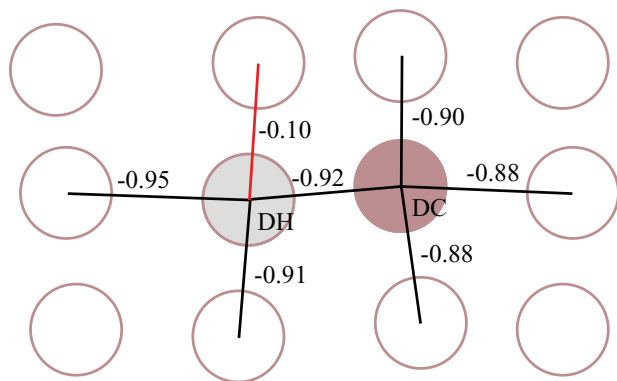


FIG. 9. Schematic description of the criteria that require four connections for defining solid-like particles. The values of  $c_{ij}$  are displayed next to the bonds that the two central particles form. The particle on the left has three bonds with  $c_{ij} < -0.87$  and one bond with  $-0.3 < c_{ij} < 0.1$ , registering it as a DH particle. The particle on the right has four bonds with  $c_{ij} < -0.87$ , registering it as a DC particle. In the mixed four-connection case, both particles would be considered solid-like.

these four connections must satisfy either the criterion for a DC particle or the criterion for a DH particle. The cartoon in Fig. 9 provides a graphical explanation of the criteria for identifying solid-like particles.

In Fig. 10, we show the barrier profile results at  $T = 0.144$  with  $\cos \theta = 0.98$  for the four different definitions of solid-like particles (three-connection, pure DC, pure DH, and unbiased four-connection mixture), in order to assess if the energy barriers of the pure crystals are different from that of the mixture and to ascertain the difference between using three or four connections in the mixed case. We cannot discern any real difference in terms of the barrier height between the four criteria. This interesting observation supports the view for this short-range model that in addition to the DH and DC free energies being essentially identical, the surface tensions are also similar. Even more, if we restrict ourselves to the comparison of all criteria in which four connections are required, then not only is the barrier height identical, but (within our numerical precision) the  $n$  dependence of the barrier profile is also identical. This suggests that the pathways to crystallizing DC

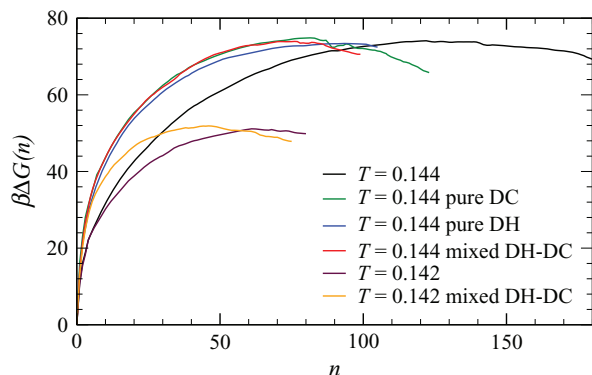


FIG. 10. Nucleation barriers for pure DC, pure DH, and mixtures of the two. For  $T = 0.144$  the four-connection curves (pure DC, pure DH, and mixed DH-DC) are all quite similar to each other and yield the same barrier height as the three-connection case, but smaller  $n^*$ . Barriers at  $T = 0.142$  compare the mixed three- and four-connection cases and confirm the invariance of  $\Delta G^*$  and the change in  $n^*$  with different criteria for defining clusters.

and DH are quite similar as well. The pure DH case appears to produce a slightly larger  $n^*$ , but this will also likely depend on the bounds on  $c_{ij}$  near  $-0.1$ . Comparing the three-connection criterion with the more restrictive four-connection cases, we see that the four-connection criterion simply results in an apparently smaller critical cluster size, providing one additional piece of evidence for the sensitivity of the profile on the solid-like definition accompanied by the insensitivity of the barrier height.

We repeat the comparison at the lower  $T = 0.142$ . However, we are unable to construct barriers for the pure DC and DH cases. At this temperature and even at moderate values of  $n_0$ , the presence of a pure DC cluster appears to act as a template for the DH growth (and vice versa). Essentially, the DH particles, which are not counted as solid-like, become part of the growing crystal, providing a bridge between only apparently different DC crystal clusters. Thus, the system crystallizes while still registering a small largest cluster in the system and our order parameter no longer describes nucleation.

This issue is greatly reduced for the four-connection mixed case and we are able to calculate the barrier at  $T = 0.142$ . Again, the barrier height is comparable to the one calculated for the case of three connections. At lower  $T$ , also for the four-connection mixed case, it becomes impossible to properly evaluate the barrier, since the overly restrictive criterion will misidentify as liquid-like particles sufficiently crystalline to participate in crystal growth.

While the barrier heights are the same across the different cluster criteria, the DC/DH composition of the clusters varies. To quantify this in a basic way, we analyze an ensemble of largest clusters extracted from a set of US simulations employing the mixed four-connection solid-like criterion in a wide range of  $n_0$  values. We find that 54% of the solid particles are DC (standard deviation 17), which is the same as the composition for clusters appearing in spontaneous nucleation studies as reported in Ref. 28. Performing the same evaluation starting from US simulations, employing this time the mixed three-connection solid-like criterion ( $q_u = -0.87$ ), the fraction of DC particles within the largest cluster is 73% (standard deviation 22). The result is the same for  $q_u = -0.65$ . This confirms that the choice of at least three connections with  $c_{ij}$  close to  $-1$  does indeed introduce a bias toward the DC structure. For this model, however, this bias does not measurably affect the nucleation barrier.

## G. Body centered cubic

For all the patch widths considered except  $\cos \theta = 0.98$  we are working in the stability field for DC/DH. For the case of  $\cos \theta = 0.98$ , the stable crystal phase at  $P = 0.03$  is the bcc (see Fig. 1), even if spontaneous nucleation indicates that the crystal that forms is the DC/DH mixture. To verify that the barrier for nucleating the bcc is significantly larger than the one for nucleating DC or DH or their mixture for  $\cos \theta = 0.98$ , we evaluate the barrier at  $T = 0.142$  using the same procedure described for the tetrahedral crystals. The definition of solid-like bcc particle is based on the  $l = 6$  spherical harmonics,<sup>8</sup> defining neighbors to be

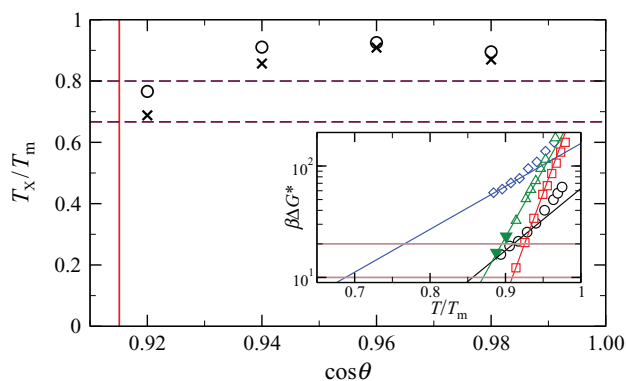


FIG. 11. Estimates of homogeneous nucleation temperature  $T_X^{10}$  (crosses) and  $T_X^{20}$  (circles) as functions of  $\cos\theta$ . The solid vertical line indicates the value of  $\cos\theta = 0.9151$  at which more than one bond per patch becomes possible for  $\delta = 0.24$ . The upper horizontal dashed line marks the approximate value of  $T_g/T_m = 0.8$  for silica, while the lower one indicates the general value of  $T_g = 2T_m/3$ . Inset shows the determination of  $T_X^{10}$  and  $T_X^{20}$  from the crossing of exponential fits to the four lowest  $T$  points for each value of  $\cos\theta$  with  $\beta\Delta G^* = 10$  and  $20$ , respectively.

connected when the scalar product of the  $l = 6$  spherical harmonics is greater than  $0.5$ . A particle is classified as solid-like if it has at least six connections. We note that Ref. 8 does not use normalized  $q_{lm}(i)$  vectors for calculating  $c_{ij}$ , so we have determined cutoffs based on our distributions of  $c_{ij}$  and of the subsequent number of connections a particle has in the liquid and in the crystal. For this state point  $\beta|\Delta\mu| = 0.866$ , while the corresponding quantity for the liquid to bcc transition is  $1.05$ . Despite this larger thermodynamic driving force, we find that the barrier to nucleating bcc is at least  $70 k_B T$  larger than that for tetrahedral crystals, supporting the lack of observation of spontaneous bcc nucleation at the pressure we consider here.

#### IV. SUMMARY AND CONCLUSIONS

Previous work for this tetrahedral patchy model showed that the driving force for nucleation (quantified as the difference in the crystal and fluid chemical potentials) decreases as the patch width increases. Figure 7 summarizes this result by showing  $\beta|\Delta\mu|$  increasing rapidly to large values as  $T$  decreases below  $T_m$  for narrow patches, while increasing only slowly and remaining fairly small for wide patches.

We find that despite this reduced driving force, the barriers to nucleation actually are smallest for the  $\cos\theta = 0.96$  [as shown in Fig. 5(a)], in the sense that this model reaches the homogeneous nucleation limit, marked, for example, by the barrier reaching a value of  $\beta\Delta G^* = 10$ , at the highest  $T/T_m$  amongst the studied models. The increased similarity between liquid and crystal in terms of energy and density as patch width increases not only brings the chemical potentials of liquid and crystal closer in value (tending to increase the nucleation barrier), but also reduces the surface tension (tending to lower the barrier). Thus, in the range of narrow angles where crystallization is readily observed, competition between  $|\Delta\mu|$  and  $\gamma$  leads to optimal nucleation, from a thermodynamic perspective, at an intermediate patch width.

Increasing the patch width beyond  $\cos\theta = 0.94$  no longer significantly reduces  $\gamma$ , while  $|\Delta\mu|$  continues to decrease, causing an increase in nucleation barrier heights. For  $\cos\theta = 0.92$ , this resulting increase is quite large, with  $\beta\Delta G^*$  estimated to be of the order of  $50$  at the lowest  $T$  that we can simulate. Moreover, the rate of decrease of  $\beta\Delta G^*$  with  $T$  appears to be quite slow, requiring significant supercooling to reach accessible nucleation barrier heights.

The evaluation of the barriers requires a definition of solid-like particles. We have checked that the barrier height is essentially insensitive to the exact choice of the cutoff used to define solid-like connections, consistent with the observation in Ref. 44 for hard-spheres. The size of the critical nucleus is instead significantly dependent on the definition of solid-like particles, again in agreement with the conclusions in Ref. 44. We have also compared several definitions of solid-like particles to probe the crystallization of a pure DC, a pure DH, and a mixed DC-DH structure. Interestingly, we find the same value of  $\beta\Delta G^*$  for all structures and, in this case, similar  $n^*$ . The fact that the entropy gain in creating a mixed structure does not appreciably lower the work of forming a critical nucleus, but is sufficient to generate a prevalence of mixed structures when spontaneous nucleation takes place,<sup>28</sup> warrants further investigation.

At this point, we would be remiss if we were not to comment on the interplay between dynamics and thermodynamics in controlling the rate of nucleation, and indeed governing the glass-forming abilities of the system. We already see an example of this within our data. The barriers at the lowest  $T$  studied for  $\cos\theta = 0.98$  and  $\cos\theta = 0.94$  are the same within error, and have a value of  $\beta\Delta G^* \approx 17$ . However, the dynamics (in terms of the diffusion coefficient) are  $40$  times slower for the wider patch case. The slow decrease in  $\beta\Delta G^*$  with  $T$ , combined with the expected further slowdown in dynamics, suggests that a search for spontaneous nucleation in unconstrained simulations would target  $T$  not far from the lowest  $T$  for which we have calculated the barrier. The case of  $\cos\theta = 0.92$  is more obvious since its dynamics are even slower at a given  $T$  than those of  $\cos\theta = 0.94$ : there is no hope of seeing nucleation in this model, which for all intents and purposes is a glass-former.

To place these results in slightly broader context, that may be illuminating for molecular tetrahedral liquids that are quite different in their glass-forming and crystallizing properties, we use the nearly exponential behavior of  $\beta\Delta G^*$  to find estimates for the temperature at which the homogeneous nucleation limit is reached,  $T_X$ . We define two such estimates using  $\beta\Delta G(T_X^{10}) = 10$  and  $\beta\Delta G(T_X^{20}) = 20$ , and determine them by fitting the lowest four points in  $T$  from Fig. 5(a) for each model to exponentials and extrapolate where necessary. In Fig. 11 we present the resulting estimates of  $T_X$  alongside a vertical line showing the widest patch that guarantees a single bond per patch, i.e., four bonds per particle. Also shown are two horizontal lines indicating the approximate value of  $T_g/T_m = 0.80$  for silica<sup>46</sup> (where  $T_g$  is the glass transition temperature), as well as the general rule of thumb  $T_g/T_m = 2/3$  (Ref. 47) which has been shown to be valid for a large class of molecular<sup>48</sup> and polymeric systems.<sup>49</sup> For  $T_X/T_m$  below  $T_g/T_m = 2/3$ , a model may be considered a

glass-former; our estimates suggest that we may be approaching this regime with our widest patch model. The presence of a maximum in  $T_X$  confirms that decreasing the angular range for bonding favors glass formation. Tetrahedral colloidal particles will thus form crystals only if the bonding angular width is small.

As a final remark, we point out that our findings may shed some light on the glass-forming and crystallizing abilities of molecular or atomic tetrahedral network-forming liquids, contributing insight as to why, for example, water crystallizes while silica more readily forms a glass.

## ACKNOWLEDGMENTS

We thank ACEnet (Canada) for computational resources. I.S.-V. acknowledges financial support from NSERC (Canada). F.S. and F.R. acknowledge support from ERC-226207-PATCHYCOLLOIDS and ITN-COMPOIDS.

- <sup>1</sup>D. Kashchiev, *Nucleation* (Butterworth-Heinemann, Oxford, 2000).
- <sup>2</sup>K. F. Kelton and A. L. Greer, *Nucleation in Condensed Matter: Applications in Materials and Biology* (Elsevier, New York, 2010).
- <sup>3</sup>P. G. Vekilov, *Soft Matter* **6**, 5254 (2010).
- <sup>4</sup>C. Vega, E. Sanz, J. L. F. Abascal, and E. G. Noya, *J. Phys.: Condens. Matter* **20**, 153101 (2008).
- <sup>5</sup>P. R. ten Wolde, M. J. Ruiz-Montero, and D. Frenkel, *J. Chem. Phys.* **104**, 9932 (1996).
- <sup>6</sup>P. R. ten Wolde, M. J. Ruiz-Montero, and D. Frenkel, *J. Chem. Phys.* **110**, 1591 (1999).
- <sup>7</sup>S. Auer and D. Frenkel, *Nature (London)* **409**, 1020 (2001).
- <sup>8</sup>S. Auer and D. Frenkel, *J. Chem. Phys.* **120**, 3015 (2004).
- <sup>9</sup>C. Valeriani, E. Sanz, and D. Frenkel, *J. Chem. Phys.* **122**, 194501 (2005).
- <sup>10</sup>J. W. Gibbs, *The Scientific Papers of J. Willard Gibbs* (Dover, New York, 1961).
- <sup>11</sup>M. Volmer and A. Weber, *Z. Phys. Chem.* **119**, 227 (1926).
- <sup>12</sup>L. Farkas, *Z. Phys. Chem.* **125**, 236 (1927).
- <sup>13</sup>R. Becker and W. Döring, *Ann. Phys.* **24**, 719 (1935).
- <sup>14</sup>K. F. Kelton, *Crystal Nucleation in Liquids and Glasses* (Academic, Boston, 1991), Vol. 45, pp. 75–177.
- <sup>15</sup>P. G. Debenedetti, *Metastable Liquids. Concepts and Principles* (Princeton University, Princeton, NJ, 1996).
- <sup>16</sup>M. Matsumoto, S. Saito, and I. Ohmine, *Nature (London)* **416**, 409 (2002).
- <sup>17</sup>M. Yamada, S. Mossa, H. E. Stanley, and F. Sciortino, *Phys. Rev. Lett.* **88**, 195701 (2002).
- <sup>18</sup>T. Motooka and S. Munetoh, *Phys. Rev. B* **69**, 073307 (2004).
- <sup>19</sup>E. Sanz, C. Vega, J. L. F. Abascal, and L. G. MacDowell, *Phys. Rev. Lett.* **92**, 255701 (2004).
- <sup>20</sup>P. Beaucage and N. Mousseau, *Phys. Rev. B* **71**, 094102 (2005).
- <sup>21</sup>E. G. Noya, C. Vega, J. P. K. Doye, and A. A. Louis, *J. Chem. Phys.* **132**, 234511 (2010).
- <sup>22</sup>L. M. Ghiringhelli, C. Valeriani, E. J. Meijer, and D. Frenkel, *Phys. Rev. Lett.* **99**, 055702 (2007).
- <sup>23</sup>L. M. Ghiringhelli, C. Valeriani, J. H. Los, E. J. Meijer, A. Fasolino, and D. Frenkel, *Mol. Phys.* **106**, 2011 (2008).
- <sup>24</sup>F. H. Stillinger and T. A. Weber, *Phys. Rev. B* **31**, 5262 (1985).
- <sup>25</sup>V. Molinero, S. Sastry, and C. A. Angell, *Phys. Rev. Lett.* **97**, 075701 (2006).
- <sup>26</sup>T. Li, D. Donadio, L. M. Ghiringhelli, and G. Galli, *Nat. Mater.* **8**, 726 (2009).
- <sup>27</sup>M. Maldovan and E. L. Thomas, *Nat. Mater.* **3**, 593 (2004).
- <sup>28</sup>F. Romano, E. Sanz, and F. Sciortino, *J. Chem. Phys.* **134**, 174502 (2011).
- <sup>29</sup>N. Kern and D. Frenkel, *J. Chem. Phys.* **118**, 9882 (2003).
- <sup>30</sup>W. Ostwald, *Z. Phys. Chem.* **22**, 289 (1897).
- <sup>31</sup>R. A. van Santen, *J. Phys. Chem.* **88**, 5768 (1984).
- <sup>32</sup>P. R. ten Wolde and D. Frenkel, *Phys. Chem. Chem. Phys.* **1**, 2191 (1999).
- <sup>33</sup>D. Frenkel and B. Smit, *Understanding Molecular Simulation: From Algorithms to Applications* (Academic, San Diego, 1996).
- <sup>34</sup>F. Romano, E. Sanz, and F. Sciortino, *J. Chem. Phys.* **132**, 184501 (2010).
- <sup>35</sup>P. J. Steinhart, D. R. Nelson, and M. Ronchetti, *Phys. Rev. B* **28**, 784 (1983).
- <sup>36</sup>J. Wedekind, R. Strey, and D. Reguera, *J. Chem. Phys.* **126**, 134103 (2007).
- <sup>37</sup>J. Wedekind and D. Reguera, in *Proceedings of the 17th International Conference on Kinetic Reconstruction of the Nucleation Free Energy Landscape in Nucleation and Atmospheric Aerosols*, Galway, Ireland, 13–17 August 2007 (Springer, Netherlands, 2008).
- <sup>38</sup>J. Wedekind and D. Reguera, *J. Phys. Chem. B* **112**, 11060 (2008).
- <sup>39</sup>G. Chkonia, J. Wlk, R. Strey, J. Wedekind, and D. Reguera, *J. Phys. Chem. B* **130**, 064505 (2009).
- <sup>40</sup>S. E. M. Lundrigan and I. Saika-Voivod, *J. Chem. Phys.* **131**, 104503 (2009).
- <sup>41</sup>I. Saika-Voivod, P. H. Poole, and R. K. Bowles, *J. Chem. Phys.* **124**, 224709 (2006).
- <sup>42</sup>W. Lechner, C. Dellago, and P. G. Bolhuis, *Phys. Rev. Lett.* **106**, 085701 (2011).
- <sup>43</sup>S. Ryu and W. Cai, *Phys. Rev. E* **81**, 030601(R) (2010).
- <sup>44</sup>L. Filion, M. Hermes, R. Ni, and M. Dijkstra, *J. Chem. Phys.* **133**, 244115 (2010).
- <sup>45</sup>Here,  $\Delta\mu$  refers specifically to the difference in chemical potential between the DC crystal and the fluid, as calculated in Ref. 28, even in the case of  $\cos\theta = 0.98$ , where the stable phase is bcc.  $T_m$  is determined from the condition  $\Delta\mu = 0$ .
- <sup>46</sup>We have used  $T_g = 1450$  K and  $T_m = 1823$  K for quartz.
- <sup>47</sup>P. G. Debenedetti and F. H. Stillinger, *Nature (London)* **410**, 259 (2001).
- <sup>48</sup>S. Sakka and J. D. Mackenzie, *J. Non-Cryst. Solids* **6**, 145 (1971).
- <sup>49</sup>W. A. Lee and G. J. Knight, *Br. Polym. J.* **2**, 73 (1970).